Research Article

Journal of RAMAN SPECTROSCOPY

Received: 4 January 2012 Accepted: 4 January 2012 Published online in Wiley Online Library

(wileyonlinelibrary.com) DOI 10.1002/jrs.4064

Rapid identification of heterogeneous mixture components with hyperspectral coherent anti-Stokes Raman scattering imaging

Erik T. Garbacik,[a] Jennifer L. Herek,[a] Cees Otto[b] and Herman L. Offerhaus[a]*

For the rapid analysis of complicated heterogeneous mixtures, we have developed a method to acquire and intuitively display hyperspectral coherent anti-Stokes Raman scattering (CARS) images. The imaging is performed with a conventional optical setup based around an optical parametric oscillator. Color coding each frame of the resulting hyperspectral data cube according to vibrational frequency results in a two-dimensional projection wherein each compound appears with a unique hue. We demonstrate the capabilities of this system by recording a hyperspectral CARS data stack of a heterogeneous mixture composed of seven crystalline amino acids and subsequently identifying each of them by direct visual analysis of the colored projection. Copyright © 2012 John Wiley & Sons, Ltd.

Keywords: Raman spectroscopy; microscopy; CARS; hyperspectral

Introduction

As a tool for chemically selective imaging, the coherent anti-Stokes Raman scattering (CARS) microscope has shown great promise in a wide range of applications, from biomedical investigations at the subcellular level[1] to the study of pharmaceutics[2] to the real-time detection of bacteria[3]. Many of the advances in CARS microscopy over the past 10 years focus on suppressing or eliminating the persistent non-resonant background that often plagues CARS experiments, especially when the concentration of resonant molecules is low[4–10]. Unfortunately, the complexity of these background-free techniques has been a significant hurdle to widespread implementation. More recently, there has been a steady increase in the use of multispectral CARS microscopy, where multiple images are obtained at selected frequencies, manually colored for maximum contrast, and overlaid in a single image[11,12]. The rapid acquisition of full spectral information at each point in a sample, known as hyperspectral imaging, is already widely used with spontaneous Raman microspectroscopy[13,14] and has long been an intrinsic goal of broadband CARS schemes[15–18]. It is only in the past few years that hyperspectral imaging has caught on with users of narrowband sources.

Narrowband hyperspectral CARS imaging has already been demonstrated with high-speed wavelength-swept laser sources[19] and optical parametric oscillators (OPOs)[20,21]. However, the former work required long pixel dwell times that could potentially lead to photodamage of fragile materials, whereas the latter reported very lengthy acquisition times for the full hyperspectral image. Further, the representation of the three-dimensional hyperspectral data is a thorny issue: the most common methods of data visualization are to either show the entire field of view at one particular frequency (akin to multispectral imaging), to extract and plot the spectra of individual pixels within the image, or to display a cross-sectional slice of the stack. Although often intuitive, none of these depictions represent *all* of the data available from the hyperspectral set, and the limitation of data can lead to misinterpretation of the results.

In this manuscript, we describe a fast hyperspectral CARS imaging method using a conventional optical setup that can be easily tailored for a wide variety of applications. To represent this data, we have also designed a technique for color coding the hyperspectral data cube as a function of frequency and then projecting the entire cube into two dimensions. The resulting projection shows the entire field of view with each compound distinguished by a different color. We demonstrate this combination of imaging and representation methods on a complicated heterogeneous mixture of pure amino acids.

Experimental details

Optical setup

Our CARS system is based around a frequency-doubled picosecond mode locked Nd:YVO_4, laser (Coherent Paladin) synchronously pumping an optical parametric oscillator (APE Berlin Levante Emerald). The signal output of the OPO, continuously tunable from 700–1000 nm, and the laser fundamental at 1064 nm are individually expanded with telescopes

* *Correspondence to: Herman L. Offerhaus, Optical Sciences group, MESA+ Institute for Nanotechnology, University of Twente, 7500AE Enschede, the Netherlands*
E-mail: h.l.offerhaus@utwente.nl

a *Optical Sciences group, MESA+ Institute for Nanotechnology, University of Twente, 7500AE Enschede, Netherlands*

b *Medical Cell BioPhysics group, MIRA Institute for Biomedical Technology and Technical Medicine, University of Twente, 7500AE Enschede, Netherlands*

and combined on a dichroic mirror. Temporal overlap is achieved with a delay stage in the 1064 nm beam. The beams are launched into a beam-scanning inverted microscope (Olympus IX71 with FluoView300 scan unit) and focused on the sample with a 40×0.9NA air objective. The power of the laser fundamental on the sample is 30 mW, whereas the maximum signal power is 50 mW and decreases as the OPO is tuned away from its gain maximum. Backscattered CARS signals are collected with the focusing objective, reflected off of a dichroic mirror, spectrally filtered, and detected with a Photo Multiplier Tube (PMT) (Hamamatsu R3986). Forward scattered CARS signals are not detected in this experiment.

For hyperspectral imaging, the crystal temperature and cavity length of the OPO are fixed, and only the angle of the intracavity Lyot filter is adjusted. By operating in this mode, we trade spectral bandwidth for higher spectral resolution, less technical complexity, and more automation than other reports of OPO-based hyperspectral CARS[20,21]. Each frame of the hyperspectral stack is recorded at a different position of the Lyot filter; the frequency interval between frames is a variable from 0.7 cm^{-1} to 100 cm^{-1} at 800 nm. For all experiments in this paper, we scan over the range 2880–3020 cm^{-1} with 2-cm^{-1} intervals. The Lyot filter movements are synchronized to the FV300 scan unit by the use of Transistor Transistor Logic (TTL) signals. The FV300 produces two pairs of digital output trigger signals when in use, one each for the vertical and horizontal galvano mirrors. These outputs indicate whether each mirror is moving in the *imaging* or *return* direction, and the two outputs for each mirror are exactly out of phase with each other. We monitor the vertical TTL output with a home-built LabVIEW program; the program idles when the TTL signal is High (HI) (indicating that the image is being recorded) and quickly switches the OPO Lyot filter to its next position when that output goes Low (LO). The power and wavelength of the OPO signal beam are recorded for each frame of the hyperspectral stack.

Hyperspectral projection

The hyperspectral data cube that we record contains two spatial dimensions and one spectral dimension. To generate the final projection, we perform three sequential steps. First, every pixel in the data cube is normalized, so that full saturation will yield a pixel value of unity, whereas a fully dark pixel will be zero. Second, each frame is assigned a value from a color look-up table (LUT). Every pixel within that frame then has a hue determined by the LUT and a color value scaled by its (normalized) intensity. The final step is the additive mixing of all frames at each spatial location with a maximum intensity method. The resulting color of each pixel qualitatively represents the spectral characteristics of the sample at that location. Sharp peaks in the spectrum will result in a bold pixel color, whereas broad spectral features will appear more white or grey. The projection method is illustrated in Fig. 1 and is implemented both within a home-built LabVIEW program and as a set of plug-ins from the McMasters Biophotonics Facility, Ontario (MBF) library for ImageJ.

Because the choice of color LUT is arbitrary and does not affect the underlying data, it is useful to choose LUTs that maximize contrast of the final image. When recording hyperspectral images of known compounds, the LUT can be carefully tailored to emphasize the most prominent spectral features so that each compound appears predictably and unambiguously. However, in many cases, it is not fully known *a priori* what materials are present in the imaged region. In these situations, the most practical LUT is one that contains the entire visible spectrum, with the primary colors equally

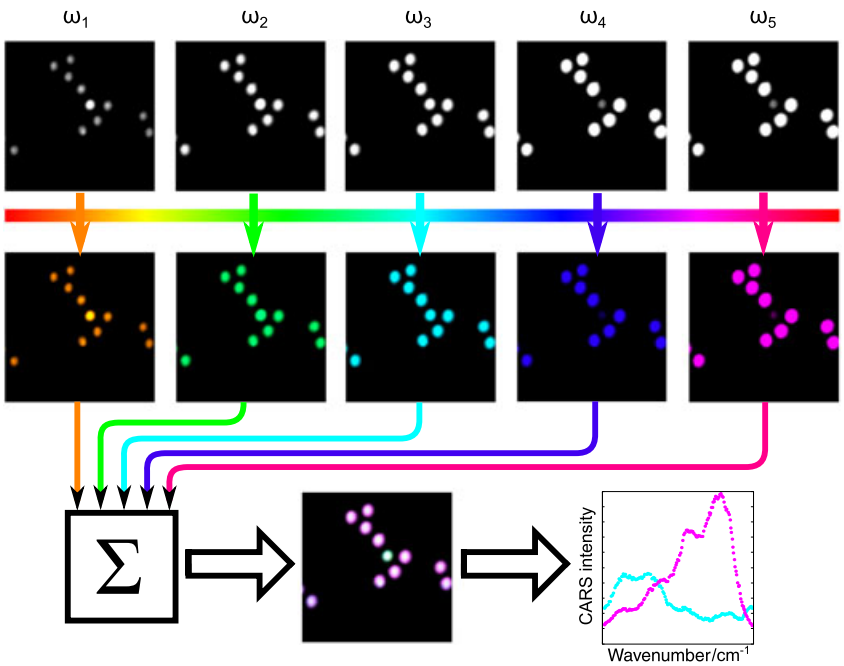

Figure 1. The hyperspectral projection method. First, a stack of images at different frequencies is recorded (top). Second, each frame is assigned a unique color according to a look-up table (middle). Third, each pixel is averaged across all frames to provide the final projected image (bottom-left). The coherent anti-Stokes Raman scattering spectrum from any given region can be extracted from the hyperspectral data set (bottom-right).

Journal of RAMAN SPECTROSCOPY

spaced. A deficiency of this LUT is that a mixture of primary colors (blue and green, for example) can appear identical to an individual secondary color (cyan). To mitigate this effect, we generate hyperspectral projections with three separate LUTs. In addition to the full-spectrum LUT described earlier, we use an LUT that repeats the spectrum twice and a further LUT that repeats the full visible spectrumalmost three times across the hyperspectral stack. These three LUTs are shown and applied to the hyperspectral images of methionine (Met) in Fig. 2. When three LUTs are used, the likelihood of two compounds sharing the same color in all of the projected images becomes very small, even when their spectra are similar. Importantly, small variations in power, step size, and start and end frequencies can result in dramatic differences in the colors of the final projection. For this reason, care is taken to ensure that every hyperspectral data set is recorded over the same frequency range.

Sample preparation

Pure (>98%) amino acids – glutamine (Gln), histidine (His), isoleucine, Met, phenylalanine (Phe), threonine (Thr), and valine – were obtained from Sigma-Aldrich and used without further chemical processing. These seven amino acids were chosen because they each exist predominantly in one physical crystalline form and because the intensities of their CARS emissions are similar. Control hyperspectral images of the individual compounds were recorded of the pure amino acids without physical processing. For the mixed samples, a few milligrams of each of the amino acids were combined together and gently ground until the average particle size was observed under a white-light inspection microscope to be less than 100 μm. The mixed sample was then sealed between two clean cover glasses to prevent oxidation and hydration.

Results and discussion

To calibrate the optical setup and hyperspectral projections, we first imaged each of the seven pure amino acids. These hyperspectral stacks contained 256 × 256 spatial pixels and 67 frequency intervals. Individual frames were recorded in 1.6 s (25 μs pixel dwell time) and averaged twice to reduce noise. For each amino acid, a composite of three hyperspectral projections is shown in Fig. 3 using the three different LUTs as described earlier.

The CARS spectra of the seven amino acids are plotted in Fig. 3 (bottom). These spectra were extracted directly from the hyperspectral data set, corrected for changes in the power of the OPO signal beam and normalized to provide a qualitative comparison of peak locations. A powerful aspect of the hyperspectral projection we use is that small differences in the CARS spectra of different compounds lead to quite striking color representations. Although His and Thr have principal peaks at nearly the same frequency (2932 and 2940 cm^{-1}, respectively), the signal appearing in the Thr spectrum at 3020 cm^{-1} results in the two compounds appearing uniquely. Even when the two compounds have nearly identical spectra, as in the case of Gln and Phe, the slight variations provide a color difference that is recognizable by eye: the third Phe projection appears bluer than that of the Gln.

The power of this projection method is best illustrated in the case of a mixture containing all seven amino acids. The prior calibration of the individual compounds makes it possible to precisely identify them directly by color. A hyperspectral image of 512 × 512 pixels was measured in 300 s (1.1 s per frame, four frames averaged together per frequency) over the same frequency range and projected with the same LUTs as previously mentioned (Figs. 4(a–c)). All of the readily identifiable crystals have been indicated monochromatically in Fig. 4(d) based on visual comparison with the calibration images. The CARS spectra extracted from these components are shown in Fig. 4(e) and agree very well with the CARS spectra measured from the pure substances (from Fig. 3, overlaid in Fig. 4(f)). The colors assigned each spectral curve in Figs. 4(e) and (f) are associated with those of the regions in Fig. 4(d). Slight differences between the two sets of spectra could be caused by a number of effects, such as re-orientation of the crystals or microscopic phase transitions due to grinding.

One drawback of this projection technique is that the colors in the hyperspectral image may not be uniform across the field

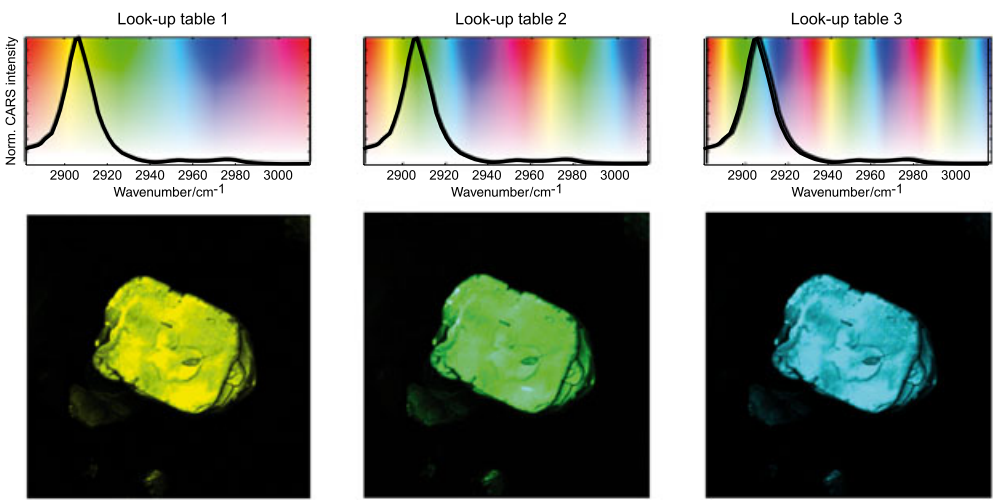

Figure 2. The three look-up table s used in this paper are applied to the hyperspectral projection of a single methionine crystal. The single prominent methionine peak yields a brilliant color in the projection image that corresponds to a narrow color band in the look-up table.

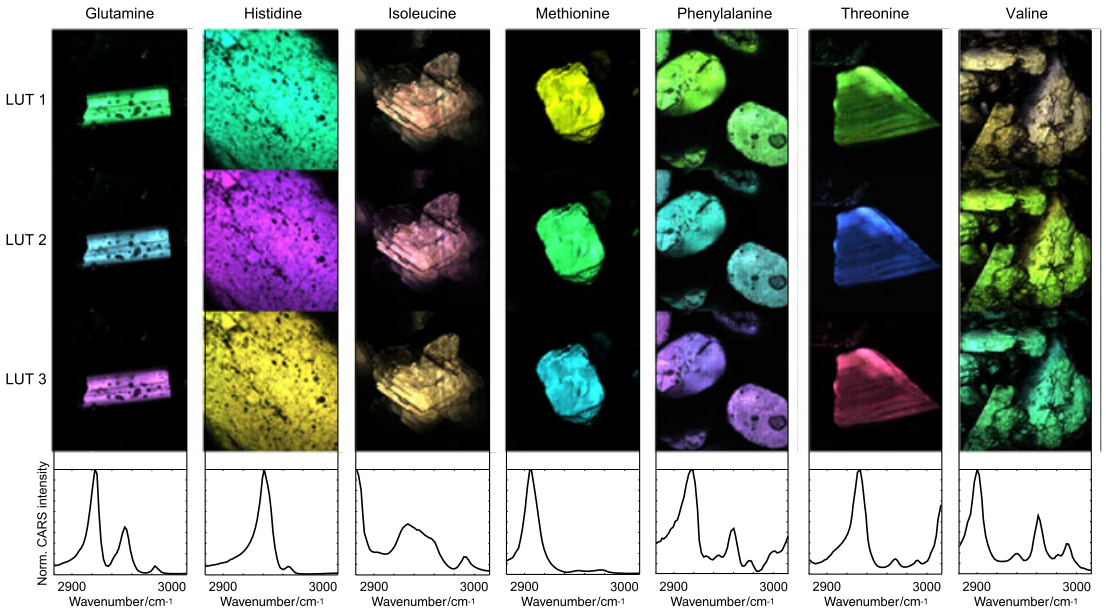

Figure 3. Top: Hyperspectral projections of seven amino acids with each of the three look-up tables. All images are 150 × ?150? μm. Bottom: Normalized coherent anti-Stokes Raman scattering spectra of the seven amino acids, directly extracted from the hyperspectral stack.

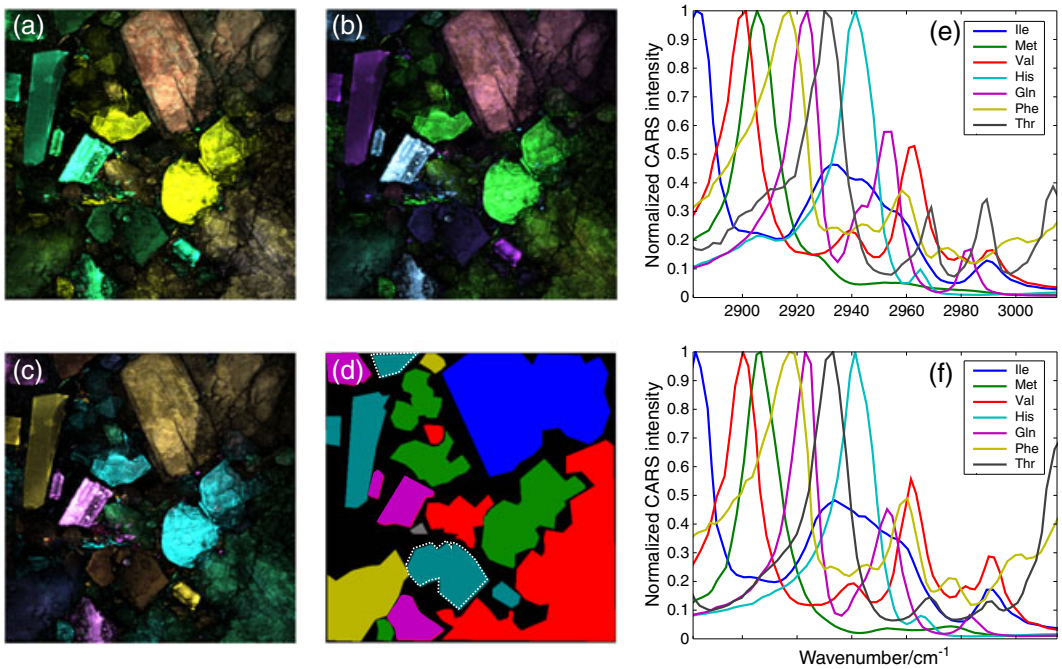

Figure 4. (a–c) Hyperspectral projections of a mixture of the seven amino acids with each of the three look-up table s. All images are 150 × ?150? μm. (d) Each identifiable crystal in (a–c) is assigned a unique color after visual comparison with the calibration images in Fig. 3. (e) Coherent anti-Stokes Raman scattering spectra extracted from each region in (d), associated to each location by color. (f) The spectra of the pure amino acids from Fig. 3, reproduced and overlaid here, show good agreement with those shown in (e).

of view for the same compound. The two crystals with dotted boundaries in Fig. 4(d) could not be identified by visual comparison with the calibration images in Fig. 3. However, comparison of the spectra (Fig. 5) revealed that these crystals share the same spectral features as His, in particular, a single strong peak near 2940cm^{-1}. Compared with the His calibration, the spectrum from the dotted region in Fig. 4(d), this peak, is slightly shifted (by approximately 3 ?cm^{-1} to a lower frequency and has a lower ratio of resonant to non-resonant contributions. Analysis of the other materials that came into contact with the sample yielded no other spectra that match with the His curve. We have observed that the His crystals are highly scattering and display birefringence by transmitting light through crossed polarizers. We believe that the peak shift may

Journal of RAMAN SPECTROSCOPY

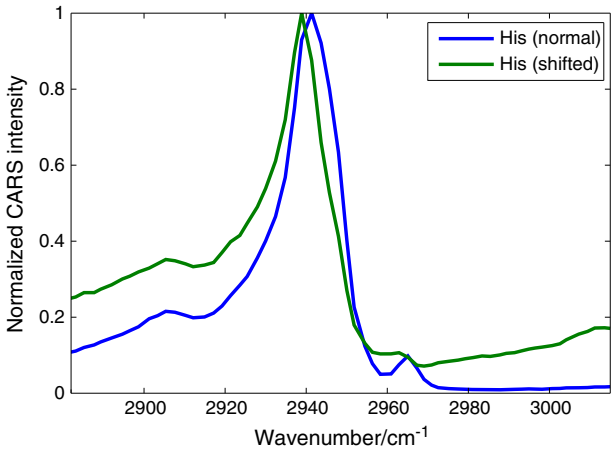

Figure 5. Comparison of shifted histidine spectrum (green, from dotted region in Fig. 4(d)) with the calibrated spectrum from Fig. 3 (blue).

be an interference because of the orientation of the crystal and optical fields[22] or as a result of material anisotropy[23,24], though a detailed study is beyond the scope of this manuscript.

Conclusion

We have demonstrated a fast method for recording and displaying hyperspectral CARS data sets using a conventional and widely used optical setup. Application of color LUTs to the spectral dimension of these data sets allows a projection to intuitively display the entire data cube in a single image, paving the way for rapid, chemically selective visual analysis of samples. In principle, this projection method could be applied to any hyperspectral data set, such as those from spontaneous Raman scattering experiments.

Acknowledgements

Funding was provided by a Vici grant to Prof. Jennifer Herek from the Nederlandse Organisatie voor Wetenschappelijke Onderzoek (NWO) and by the Stichting voor Fundamenteel Onderzoek der Materie (FOM). We are grateful to Coherent Inc. for use of the Paladin laser and to APE Berlin for the Levante Emerald OPO.

Reference

[1] C. Brackmann, J. Norbeck, M. Åkeson, D. Bosch, C. Larsson, L. Gustafsson, A. Enejder, *J. Raman Spectrosc.* **2009**, *40*, 748.
[2] M. Windbergs, M. Jurna, H. L. Offerhaus, J. L. Herek, P. Kleinebudde, C. J. Strachan, *Anal. Chem.* **2009**, *81*, 2085.
[3] D. Pestov, X. Wang, G. O. Ariunbold, R. K. Murawski, V. A. Sautenkov, A. Dogariu, A. V. Sokolov, M. O. Scully, *Proc. Nat. Acad. Sci.* **2008** *105*, 422.
[4] J.-X. Cheng, A. Volkmer, X. S. Xie, *J. Opt. Soc. Am. B* **2002**, *19*, 1363.
[5] A. Volkmer, L. D. Book, X. S. Xie, *Appl. Phys. Lett.* **2002**, *80*, 1505.
[6] E. O. Potma, C. L. Evans, X. S. Xie, *Opt. Lett.* **2006**, *31*, 241.
[7] F. Lu, W. Zheng, C. Sheppard, Z. Huang, *Opt. Lett.* **2008**, *33*, 602.
[8] C. Mueller, T. Buckup, B. von Vacano, M. Motzkus, *J. Raman Spectrosc.* **2009**, *40*, 809.
[9] M. Jurna, J. P. Korterik, C. Otto, J. L. Herek, H. L. Offerhaus, *Phys. Rev. Lett.* **2009**, *103*, 043905.
[10] K. Orsel, E. T. Garbacik, M. Jurna, J. P. Korterik, C. Otto, J. L. Herek, H. L. Offerhaus, *J. Raman Spectrosc.* **2010**, *41*, 1678.
[11] C. Brackmann, A. Bengtsson, M. L. Alminger, U. Svanberg, A. Enejder, *J. Raman Spectrosc.* **2011**, *42*, 586.
[12] J. Rehbinder, C. Pohling, T. Buckup, M. Motzkus, *Opt. Lett.* **2010**, *35*, 3721.
[13] Y.-S. Huang, T. Karashima, M. Yamamoto, H.-o. Hamaguchi, *Biochem.* **2005**, *44*, 10009.
[14] V. V. Pully, A. T. M. Lenferink, C. Otto, *Spectrosc.* **2011**, *42*, 167.
[15] R. Selm, M. Winterhalder, A. Zumbusch, G. Krauss, T. Hanke, A. Sell, A. Leitenstorfer, *Opt. Lett.* **2010**, *35*, 3282.
[16] A. C. W. van Rhijn, H. L. Offerhaus, P. van der Walle, J. L. Herek, A. Jafarpour, *Opt. Express* **2010**, *18*, 2695.
[17] C. Pohling, T. Buckup, M. Motzkus, *J. Biomed. Opt.* **2011**, *16*, 021105.
[18] Y. J. Lee, D. Moon, K. B. Migler, M. T. Cicerone, *Anal. Chem.* **2011**, *83*, 2733.
[19] S. Bégin, B. Burgoyne, V. Mercier, A. Villeneuve, R. Vallée, D. Côté, *Biomed. Opt. Express* **2011**, *2*, 1296.
[20] C.-Y. Lin, J. Suhalim, C. L. Nien, M. Miljkovic, M. Diem, J. Jester, E. Potma, *J. Biomed. Opt.* **2011**, *16*, 021104.
[21] S. Brustlein, P. Ferrand, N. Walter, S. Brasselet, C. Billaudeau, D. Marguet, H. Rigneault, *J. Biomed. Opt.* **2011**, *16*, 021106.
[22] C. H. Raymond Ooi, *J. Raman Spectrosc.* **2009**, *40*, 714.
[23] G. Lucassen, Polarization sensitive coherent Raman spectroscopy on (bio)molecules in solutions, Ph.D. thesis, University of Twente, **1992**.
[24] F. Munhoz, Polarization resolved four-wave mixing microscopy: structural and vibrational read-out in molecular media, Ph.D. thesis, Universite Paul Cezanne - Aix Marseille, **2010**.